Results from the PHENIX experiment at RHIC

H. Pereira Da Costa[1] for the PHENIX collaboration

[1]Dapnia, CEA Saclay, F-91191, Gif-sur-Yvette, France

E-mail: pereira@hep.saclay.cea.fr

Abstract. This contribution presents recent results from the PHENIX experiment at RHIC in Au+Au, Cu+Cu and p+p collisions. Emphasis is given on light quarks, heavy quarks and gluons energy loss, elliptic flow, particle correlations, and di-lepton measurements.

1. Introduction

The heavy ion program pursued at the Relativistic Heavy Ion Collider (RHIC) aims to identify and study the formation of a possible quark-gluon plasma in ultra-relativistic heavy ion collisions, a state of nuclear matter in which the quarks and gluons evolve freely on distances larger than the typical nucleon size. PHENIX has made a number of measurements that, taken together, strongly indicate that the matter created in heavy ion collisions is indeed hot and dense and has properties which differ significantly from normal (cold) nuclear matter: a suppression of hadrons with large transverse momentum (p_T) is observed, characterized by a nuclear modification factor $R_{\rm AA}$ smaller than unity, in contrast to direct photons; scaling properties observed for the elliptic flow v_2 of a large variety of particles indicate the existence of pre-hadronic degrees of freedom in the medium; azimuthal correlations between particles produced in the collision reveal strong interactions of hard-scattered partons with the bulk of the medium; a significant suppression observed for high p_T charmed hadrons indicates high medium density, short relaxation time and/or small diffusion coefficient for heavy quarks. This presentation reviews recent results from the PHENIX experiment in p+p, Cu+Cu and Au+Au collisions that aim to study the effects listed above in more detail. Some of the PHENIX contributions to this conference could not be detailed in this review; please refer to the corresponding proceedings [1, 2, 3].

2. Energy loss

The nuclear modification factor $R_{\rm AA}$ is the ratio between a given particle production yield in heavy ion collisions and its counterpart in p+p collisions, normalized by $N_{\rm coll}$, the average number of equivalent nucleon-nucleon collisions at a given centrality. For particles whose production is dominated by the scattering of partons with large momentum transfer, the particle yield is expected to scale with $N_{\rm coll}$ (leading to $R_{\rm AA} = 1$) in absence of medium effects. Such conditions are fulfilled for high p_T (> 2 GeV/c) hadrons and for so-called *direct* photons, defined as all photons produced during the collision that do not originate from radiative decay. Direct photons are

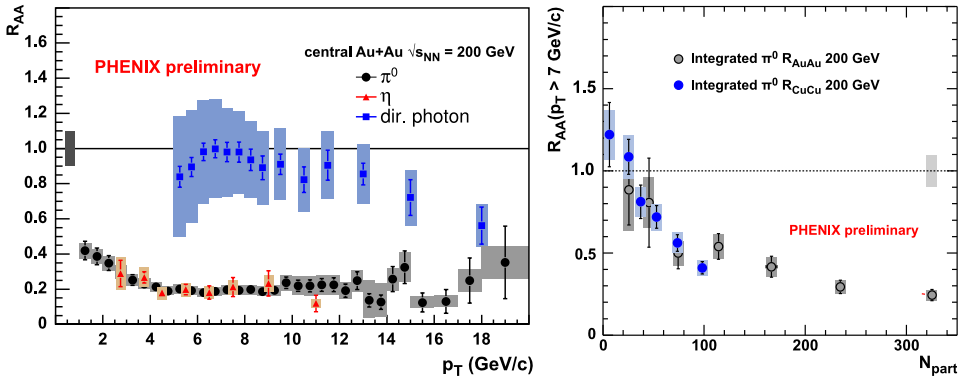

Figure 1. Left: direct photon and π^0 $R_{\rm AA}$ as a function of p_T in central gold-gold collisions at $\sqrt{s_{\rm NN}}$ = 200 GeV; right: π^0 $R_{\rm AA}$ as a function of $N_{\rm part}$ in copper-copper and gold-gold collisions at $\sqrt{s_{\rm NN}} = 200$ GeV.

derived from inclusive photon spectra after subtraction of all background sources (primarely from π^0 and η decays).

Figure 1 (left) shows $R_{\rm AA}$ for π^0, η and direct photons in central Au+Au collisions at $\sqrt{s_{\rm NN}}$ = 200 GeV, up to p_T = 20 GeV/c. For $p_T > 4$ GeV/c, the π^0 $R_{\rm AA}$ is essentially flat and close to 0.2, consistent with earlier results from PHENIX [4]. The same suppression is observed for η's, which indicates that the quenching mechanism does not depend on the particle mass and occurs at the partonic level prior to fragmentation/coalescence. For direct photons, $R_{\rm AA}$ is compatible with unity for $p_T < 13$ GeV/c as in [5]. This rules out explanations of the observed π^0 suppression via modifications of parton distribution functions since direct photons traverse the produced medium basically unaffected but would be sensitive to such modifications. For $p_T > 13$ GeV/c a suppression is observed which has been attributed to the fact that for high enough p_T the contribution of valence quarks to direct photon production becomes non-negligible and induces a distinction between protons and neutrons that does not cancel when forming $R_{\rm AA}$. If this explanation is valid, measurements performed at a lower energy should show the same effect, but starting at a lower p_T.

The π^0 $R_{\rm AA}$ was also measured for Cu+Cu collisions at the same energy. The right panel of Figure 1 shows that the centrality dependence of $R_{\rm AA}$ for both systems is the same within errors. Some calculations predict a slight modification of the slope due to the difference in the geometry of the overlapping region between the two systems and the interplay between volume and surface effects on the suppression [6]. So far, the accuracy of the data does not allow confirmation or rejection of such predictions.

$R_{\rm AA}$ was also measured for light mesons (ϕ and ω) in d+Au and Au+Au collisions [7]. In d+Au collisions measured ϕ and ω $R_{\rm AA}$ are consistent with unity, although the measurement uncertainty is too large to firmly quantify possible cold nuclear matter effects. In central Au+Au collisions a suppression is observed that is similar to the π^0 measurement, but with even larger uncertainties. Additionally, no modification of the mass or width of these mesons was observed so far.

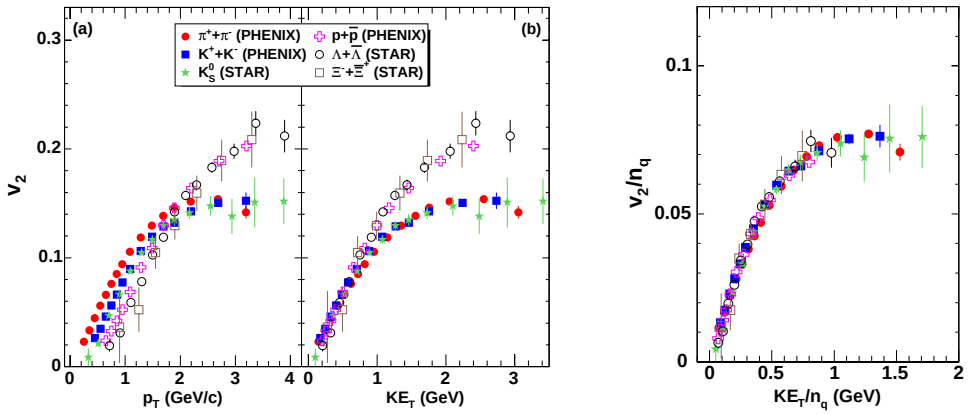

Figure 2. Left: elliptic flow (v_2) for identified hadrons vs p_T; middle: v_2 vs KE_T; right: v_2/n_q vs KE_T/n_q.

3. Elliptic flow

The magnitude of the elliptic flow (v_2) characterizes the azimuthal anisotropy of particle emission with respect to the collision reaction plane. A positive v_2 was observed in Au+Au mid-central and central collisions, meaning that particles are emitted preferentially in the direction perpendicular to the reaction plane. This property is interpreted as evidence for an anisotropic pressure gradient in the overlap region of colliding nuclei. Measured v_2 values are well reproduced by hydrodynamic models, provided that the viscosity of the medium is small.

PHENIX has measured v_2 for charged mesons in Cu+Cu and Au+Au collisions in four centrality bins ranging from 0 to 40% [8]. As expected, v_2 is smaller for more central collisions, as the overlapping region becomes more spherical. When dividing v_2 at a given p_T by its integral over p_T, the values fall on the same curve for both systems and all centrality bins. This indicates that the p_T dependence of v_2 for a given particle is universal whereas its magnitude is driven by the geometry of the overlapping region only.

Figure 2 shows the elliptic flow of several hadrons measured by both the PHENIX [8] and STAR [9, 10] collaborations in minimum bias Au+Au collisions. Several variables are used for the horizontal and vertical axis in order to highlight different scaling properties. The left panel shows v_2 as a function of the particle p_T. For $p_T \lesssim 2.5$ GeV/c, the values are ordered by the particle mass, with a larger v_2 for light particles. This effect cancels when using the particle transverse kinetic energy $KE_T = m_T - m$ (with m_T the transverse mass of the particle) in place of p_T for the x axis. For $p_T \sim 2 - 4$ GeV/c, the v_2 of baryons and mesons are well separated, with a larger v_2 for baryons. This separation disappears when both axis are divided by the number of constituent quarks n_q. This has been attributed to the dominance of quark coalescence over fragmentation as a mechanism for particle production.

PHENIX also measured the elliptic flow of ϕ mesons and d nuclei in Au+Au collisions [11]. The ϕ meson is of special interest because its mass is of the same order as the proton mass and it has low hadronic interaction cross-sections. As for the d nucleon, its interest resides in the fact that $n_q = 6$, thus representing an extreme test

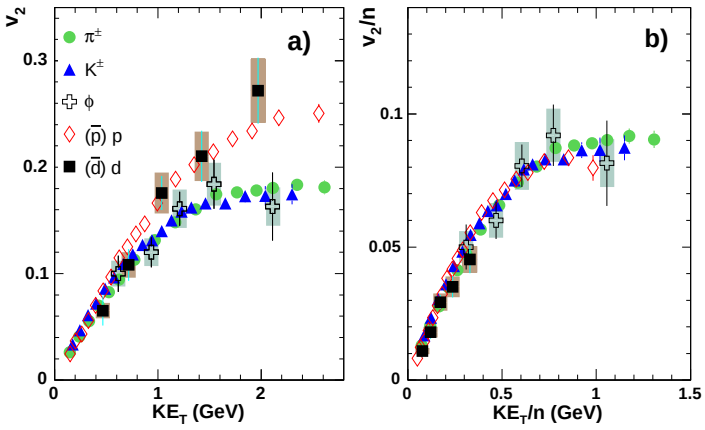

Figure 3. Left: v_2 of ϕ mesons, d nuclei and other identified hadrons vs KE_T in minimum bias Au+Au collisions at $\sqrt{s_{\rm NN}} = 200$ GeV/c; right: v_2/n_q vs $KE_{\rm T}/n_q$.

of the scaling observed in the right panel of Figure 2. As shown in Figure 3, it is found that both the ϕ and d v_2 follow the scaling properties described above, which indicates that the v_2 develops prior to hadronization and reflects the pre-hadronic (possibly partonic) degrees of freedom of the medium. For the d however, it is to be noted that the p_T extent of the measurement in not wide enough to test the KE_T/n_q scaling in the region where it is most pertinent.

4. Jet correlations

Two-particle azimuthal correlations are formed by choosing a *trigger* particle of high enough p_T and looking at the azimuthal distribution of associated particles in a given p_T range. The resulting correlation functions exhibit a so-called *near-side* peak at $\Delta\phi = 0$ characteristic of associated particles that belong to the same jet as the trigger particle and an *away-side* peak at $\Delta\phi = \pi$ corresponding to the associated jet produced back-to-back in the initial parton hard-scattering. Strong modifications of both the shape and strength of the away-side peak have been observed as illustrated in Figure 4 (left). Here the away-side peak deviates from the expected Gaussian shape and a local maximum is observed away from $\Delta\phi = \pi$. Such modifications are inferred to interaction of the initial parton with the matter produced during the collision.

Several methods have been developed to quantify the modifications of the away-side peak and its dependence on the colliding nuclei, the collision centrality and the trigger and associated particle p_T range [12, 13]. One method consists of measuring the second and fourth order moments (the RMS and the Kurtosis) of the correlation function about $\Delta\phi = \pi$. The RMS quantifies the width of the away-side peak whereas the Kurtosis K quantifies the deviation of the peak shape from a Gaussian distribution (for which $K = 3$). A second method consists of fitting the correlation function with several Gaussian distributions (one for the near side peak, and two for the away side peak in order to reproduce the observed local minimum), and using the fit result to derive a splitting parameter D that quantifies the location of the maximum with respect to $\Delta\phi = \pi$. Figure 4 (right) shows the values for the RMS, the Kurtosis

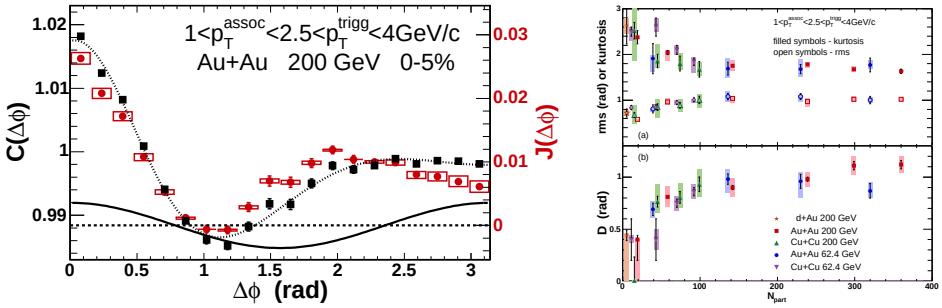

Figure 4. Left: acceptance corrected hadron-hadron azimuthal correlation function in Au+Au collisions at $\sqrt{s_{\rm NN}}$ = 200 GeV/c. Squares are for the raw correlation function; circles are for the v_2 corrected correlation function; the solid line is the estimated v_2 contribution. Right: away-side peak shape characterization variables vs $N_{\rm part}$ in Au+Au and Cu+Cu collisions at $\sqrt{s_{\rm NN}}$ = 200 and 62 GeV/c.

and the splitting parameter D versus $N_{\rm part}$ for Au+Au and Cu+Cu collisions at $\sqrt{s_{\rm NN}}$ = 200 and 62 GeV/c. All three parameters have values corresponding to a Gaussian for peripheral collisions. For more central collisions they follow a trend that depends on $N_{\rm part}$ only and not on the system size or energy. This independence, also observed with respect to the associated particle p_T, puts severe constraints on models that attempt to explain these shape modifications in terms of, for instance, a shock wave, a Mach cone, jet deflection, or Cerenkov gluon radiation. A third method to characterize the away-side peak consists of defining three $\Delta\phi$ ranges, two of them (the shoulders) corresponding to the local maximum away from π and one (the head) corresponding to the local minimum at π, then forming the ratio (head over shoulders) of the integrated correlation functions over these three ranges. A ratio greater than one is characteristic of the *normal* away-side peak shape while the shape shown in Figure 4 (left) corresponds to a ratio smaller than one[13].

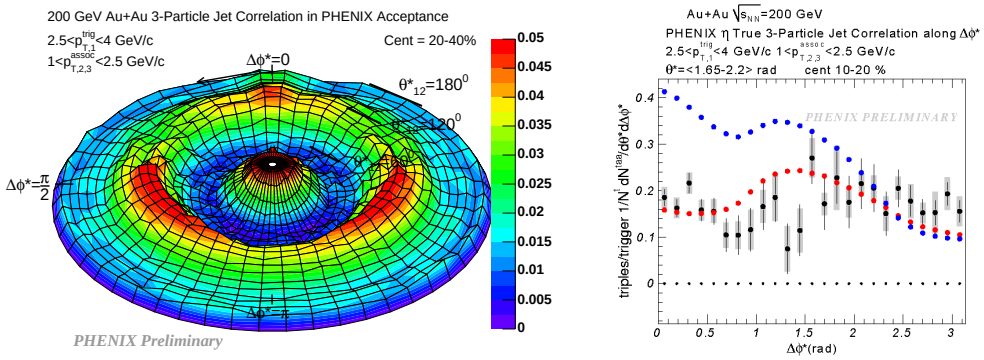

Figure 5. Three-particle correlations in Au-Au collisions at $\sqrt{s_{\rm NN}}$ = 200 GeV/c.

Three-particle correlations also provide a useful tool to disentangle possible explanations for the observed away-side peak shape modification. A high p_T trigger

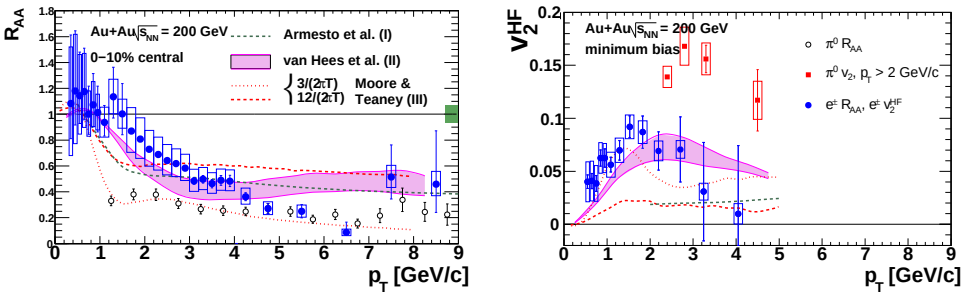

Figure 6. Left: non-photonic electron $R_{\rm AA}$ vs p_T in Au+Au central (0-10%) collisions at $\sqrt{s_{\rm NN}} = 200$ GeV; Right: non-photonic electron v_2 vs p_T in Au+Au minimum bias collisions at the same energy.

particle (p_1) is picked in the event and its momentum direction is used as the z axis. Two other particles (p_2 and p_3) are picked in a given p_T range and a correlation function is built as a function of θ^*_{12} the angle between p_1 and p_2 and $\Delta\phi^*_{23}$ the azimuth difference between p_2 and p_3. Such a correlation function is shown in polar coordinates in Figure 5 (left). The peak at the center ($\theta^* = 0$) corresponds to the near-side jet, while the *ring* at $\theta^* \gtrsim 100°$ (1.7 rad) corresponds to the away-side jet. Models predict rather different shapes for this ring: deflected jet models predict a peak at $\Delta\phi^* = 0$, whereas Mach cone models predict a more isotropic shape. These features are best illustrated by looking at the correlation function integrated over a θ range that contains the away-side peak versus $\Delta\phi^*$ (Figure 5, right). A comparison of the models to the data favors Mach cone modifications.

Finally, PHENIX has also measured correlation functions between direct photons and hadrons in p+p and Au+Au collisions. They are derived using inclusive photon-hadron correlations from which the decay photon contribution, estimated using π^0-hadron correlations, is subtracted [14]. The use of a direct photon as a trigger particle should provide a more precise energy reference than hadrons when studying the energy loss of the jet recoiling opposite to it. In p+p collisions, the measured correlation functions are compatible with expectations from PYTHIA for all trigger and associated particle p_T bins. In Au+Au collisions the results are statistically limited and do not allow firm conclusions. However, they demonstrate the feasibility of such a measurement given a large enough data set.

5. Heavy flavors

Heavy quarks are produced at the beginning of the collision via hard scattering of partons. In PHENIX they are measured indirectly using so-called *non-photonic* electrons that correspond to decay of heavy flavored mesons. Non-photonic electron yields are extracted from inclusive electron spectra after all identified background contributions (mostly from π^0 and η Dalitz decays as well as photo-conversion in the detector materials) are subtracted using the techniques described in [15].

Figure 6 (left) shows the nuclear modification factor $R_{\rm AA}$ of non-photonic electrons versus p_T in central Au+Au collisions at $\sqrt{s_{\rm NN}} = 200$ GeV/c. For $p_T < 2$ GeV/c, $R_{\rm AA}$ is consistent with unity. For larger p_T, it decreases until it reaches approximately the same level as the π^0 $R_{\rm AA}$ measured in the same conditions.

Figure 6 (right) shows the elliptic flow v_2 of non-photonic electrons as a function of p_T in minimum-bias Au+Au collisions. Also shown on both figures are calculations that attempt to simultaneously reproduce the measured $R_{\rm AA}$ and v_2 [16, 17, 18]. These calculations, although with different approaches, all require a short heavy quark relaxation time and/or a small diffusion coefficient, both of which are consistent with a QCD medium of low viscosity as is also suggested by the light quarks measurements.

6. Di-lepton continuum and heavy quarkonia

Figure 7 shows the invariant mass distribution of correlated unlike-sign electron pairs measured at mid-rapidity in p+p and Au+Au collisions at $\sqrt{s_{\rm NN}} = 200$ GeV. The identified contributions to this spectrum, estimated and normalized using the technique described in [19], are also shown on the figure. In p+p collisions the data are compatible with the simulations except in the intermediate mass range $m \in [1.5, 2.5]$ GeV. In Au+Au collisions on the other hand an excess is observed at low mass ($m < 0.7$ GeV). The same study has been performed versus centrality in Au+Au collisions. The spectrum measured in peripheral collisions (60-100%) is essentially the same as in p+p, whereas for central collisions (0-10%), an excess is observed in the low mass region similar to the one observed in the minimum-bias case.

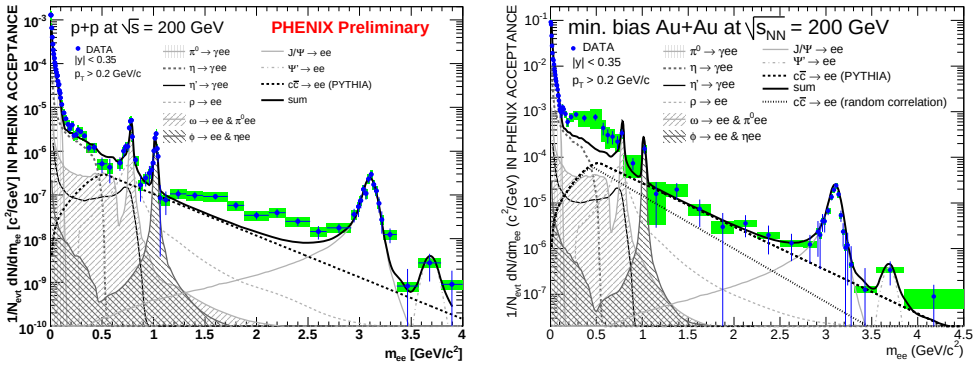

Figure 7. correlated electron pairs invariant mass distribution at mid-rapidity ($|y| < 0.35$) in p+p (left) and Au+Au (right) collisions at $\sqrt{s_{\rm NN}} = 200$ GeV.

Also visible in Figure 7 is a clear J/ψ signal at $m = 3.1$ GeV. The ability to measure J/ψ at both mid and forward rapidity is a unique feature of the PHENIX spectrometer at RHIC. J/ψ production has been measured in p+p [20] and Au+Au collisions [21] at $\sqrt{s_{\rm NN}} = 200$ GeV. The p+p data sample is about 10 times larger than for previously published results [22] and allows a precise determination of the J/ψ rapidity (and p_T) distributions (Figure 8, left). A total cross-section of $B_{ll}\sigma_{\rm pp}^{\rm J/\psi} = 178 \pm 3({\rm stat}) \pm 53({\rm sys}) \pm 18({\rm norm})$ nb is measured by fitting the J/ψ differential cross-section vs y and integrating the resulting function.

The J/ψ $R_{\rm AA}$ has been measured in Au+Au collisions vs $N_{\rm part}$ using the above p+p data as a reference (Figure 8, right). At both rapidities, $R_{\rm AA}$ decreases with increasing $N_{\rm part}$. For the most central collisions, $R_{\rm AA}$ is below 0.3 (0.2) at mid (forward) rapidity. The fact that the nuclear modification factor is consistently lower at forward rapidity than at mid-rapidity is striking since models that invoke a J/ψ

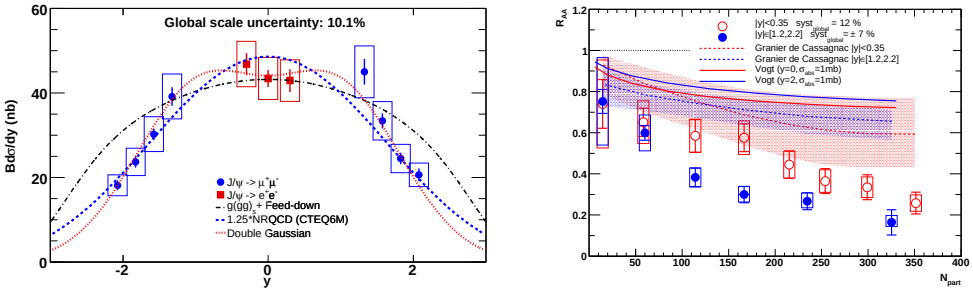

Figure 8. Left: J/ψ production cross-section as a function of rapidity in p+p collisions at $\sqrt{s_{\rm NN}} = 200$ GeV; right: J/ψ $R_{\rm AA}$ as a function of $N_{\rm part}$ at mid and forward rapidity in Au+Au collisions at the same energy.

suppression based on the medium energy density predict the opposite trend. Also striking is the fact that the measured $R_{\rm AA}$ at mid-rapidity has the same magnitude as the one measured at CERN SPS [23, 24], despite the fact that the collision energy is about 10 times larger at RHIC and that the cold nuclear matter effects (CNM) are not expected to be identical. Also shown in Figure 8 (right) are several calculations for the CNM as extrapolated from PHENIX d+Au measurements [22, 25, 26]. All calculations show a smaller suppression (a larger $R_{\rm AA}$) than the measured values. However the large error bars for both the models and the data prevent a quantitative conclusion on the magnitude and $N_{\rm coll}$ dependence of J/ψ suppression beyond expected CNM suppression.

References

[1] P. Chun. *this conference.*
[2] A. Taranenko. *this conference.*
[3] X. Wang. *this conference.*
[4] S. S. Adler et al. *Phys. Rev. Lett.*, 91:072301, 2003.
[5] S. S. Adler et al. *Phys. Rev. Lett.*, 94:232301, 2005.
[6] V. S. Pantuev. *JETP Lett.*, 85:104–108, 2007.
[7] V. Ryabov. *this conference.*
[8] A. Adare et al. *Phys. Rev. Lett.*, 98:162301, 2007.
[9] J. Adams et al. *Phys. Rev. Lett.*, 92:052302, 2004.
[10] J. Adams et al. *Phys. Rev. Lett.*, 95:122301, 2005.
[11] S. Afanasiev et al. *Phys. Rev. Lett.*, 99:052301, 2007.
[12] A. Adare et al. *Phys. Rev. Lett.*, 98:232302, 2007.
[13] A. Adare et al. *arXiv:0705.3238 [nucl-ex]*, 2007.
[14] J. Jin. *J. Phys.*, G34:S813–816, 2007.
[15] A. Adare et al. *Phys. Rev. Lett.*, 97:252002, 2006.
[16] N. Armesto et al. *Phys. Lett.*, B637:362–366, 2006.
[17] Hendrik van Hees, Vincenzo Greco, and Ralf Rapp. *Phys. Rev.*, C73:034913, 2006.
[18] Guy D. Moore and Derek Teaney. *Phys. Rev.*, C71:064904, 2005.
[19] S. Afanasiev et al. *arXiv:0706.3034 [nucl-ex]*, 2007.
[20] A. Adare et al. *Phys. Rev. Lett.*, 98:232002, 2007.
[21] A. Adare et al. *Phys. Rev. Lett.*, 98:232301, 2007.
[22] S. S. Adler et al. *Phys. Rev. Lett.*, 96:012304, 2006.
[23] M. C. Abreu et al. *Phys. Lett.*, B410:337–343, 1997.
[24] B. Alessandro et al. *Eur. Phys. J.*, C39:335–345, 2005.
[25] R. Vogt. *Acta Phys. Hung.*, A25:97–103, 2006.
[26] Raphael Granier de Cassagnac. *J. Phys.*, G34:S955–958, 2007.